Catalysis Surveys from Asia (2023) 27:132–138
https://doi.org/10.1007/s10563-022-09380-w

ORIGINAL ARTICLE

Synthesis of Solid Acid Catalysts of $MgO–Al_2O_3$ Mixed Oxide Containing Oxyanions by Thermal Decomposition of Anion-Exchanged Hydrotalcites

Hiromi Matsuhashi[1]

Received: 15 September 2022 / Accepted: 16 October 2022 / Published online: 31 October 2022

Abstract
Solid acid catalysts of $MgO–Al_2O_3$ mixed oxides containing $B_4O_7^{2-}$, HPO_4^{2-}, $Mo_7O_{24}^{6-}$, MoO_4^{2-}, WO_4^{2-}, and SO_4^{2-} were synthesized by anion exchange with Cl^- located in the space between anionic layers of hydrotalcite, followed by heat treatment at 773 K. The distance between the hydroxide layers was expanded by the intercalation of oxyanions larger than Cl^-. The exchange of oxyanions in the interlayer space was confirmed by IR spectroscopy. Acid sites were generated on the obtained mixed oxides of $MgO–Al_2O_3$ by the electron withdrawing effect of the oxyanions. The acid catalyzed ethanol dehydration into ethylene and diethyl ether took place on the obtained catalysts. The effect of exchanged anions in the generation of acid sites was the largest in SO_4^{2-}.

Keywords Hydrotalcite · Anion exchange · Solid acid

1 Introduction

Hydrotalcite (HT) is an anionic-layered double-hydroxide [1–3]. The formula of the most popular hydrotalcite, Mg–Al HT, is $Mg_6Al_2(OH)_{16}(CO_3)\cdot 4H_2O$. Mg–Al HT consists of brucite-like layers of $Mg(OH)_2$, with partial substitution of some Mg^{2+} ions with Al^{3+} ions. The excess positive charge originating from Al^{3+} is balanced by various intercalated inorganic and organic anions located between the layers along with water molecules. It is well known that anions within the interlayer can be exchanged. The stability of anions between the layers increases with increasing electric charge of the anion and decreasing anion size as follows, $CO_3^{2-} > SO_4^{2-} > OH^- > F^- > Cl^- > Br^- > NO_3^- > I^-$ [4, 5]. Conventionally, Mg–Al HT is synthesized by co-precipitation of an aqueous alkaline solution of Mg and Al salts [6]. Generally, an aqueous NaOH or KOH solution is used to adjust the pH and an aqueous Na_2CO_3 or K_2CO_3 solution is added as the carbonate source, which is intercalated in the space between layers [6]. The CO_3^{2-} anion within the interlayer is the most stable, making it difficult to exchange with other anions by simple anion exchange procedures.

Mg–Al HT has been applied as a solid base catalyst [1, 2, 7–13]. The mixed oxide obtained by thermal decomposition of HT exhibits much higher activity than the original HT [14–16]. The base strength of Mg–Al HT is from 13.3 to 16 on the pK_a scale [17], which is much lower than that of thermally decomposed HT [18] and simple MgO [19]. The MgO base catalyst modified with Al_2O_3 shows sufficient activity for a base catalyzed reaction. The basicity was not lowered by modification with Al_2O_3 [20]. The lower basicity of $MgO–Al_2O_3$ mixed oxide is considered to be due to the electron withdrawing effect of CO_3^{2-}.

The acidity of several kinds of metal oxides can be increased by introduction of sulfate ions to the hydroxide or oxide surface, followed by heat treatment at elevated temperatures [22–24]. A representative example is the sulfation of ZrO_2, where the acidity was largely increased by introducing sulfate to ZrO_2 followed by heat treatment. Tungstate, molybdate, and borate also increased the acidity of ZrO_2 [22–24].

As described above, anions located between layers are exchangeable. In this study, Mg–Al HT containing Cl^- as the interlayer anion was prepared, and then Cl^- was exchanged with borate, phosphate, molybdate, tungstate, and sulfate. The effect of anions incorporated in the bulk of $MgO–Al_2O_3$,

✉ Hiromi Matsuhashi
matsuhashi.hiromi@h.hokkyodai.ac.jp

[1] Hokkaido University of Education, Hakodate Campus, Hakodate 040-8567, Japan

prepared by the thermal decomposition of anion–exchanged Mg–Al HT, on the acidity of the solid surface was studied.

2 Experimental

2.1 Catalyst Preparation

To purge CO_2 from the distilled water used in this study, water was boiled under N_2 bubbling before use, and continuous bubbling of N_2 was performed during sample preparation. The hydrotalcite containing Cl^- as the intercalated anion was prepared by a coprecipitation method [25–27]. Magnesium chloride hexahydrate (0.75 mol) and $AlCl_3{\cdot}6H_2O$ (0.25 mol) were dissolved in 1 L of distilled water in an Erlenmeyer flask, and NaOH solution (1.0 mol L^{-1}, 1 L) was added dropwise to the mixed solution. The solution was stirred for 2 h while heating at 333 K. The precipitate was filtered, then suspended in decarbonated water, and filtered again. The obtained sample was dried in an oven at 378 K. This sample is denoted as HT–Cl.

Chloride anion intercalated in hydrotalcite was exchanged with oxyanions. The salts used for anion exchange were $Na_2B_4O_7$, HNa_2PO_4, $(NH_4)_6Mo_7O_{24}$, Na_2MoO_4, WO_3 dissolved in aqueous NH_3, Na_2WO_4 and $MgSO_4$. The salt (1.5 times mol against Al^{3+} contained in used HT–Cl) was dissolved in the decarbonated water, and the desired amount of HT–Cl was added to the solution. The solution containing the HT–Cl suspension was stirred for 1 h at room temperature, and then filtered. The precipitate was suspended in decarbonated water for washing and filtered again. Finally, the sample was dried in an oven at 378 K for one day. Anion-exchanged samples with $Na_2B_4O_7$, HNa_2PO_4, $(NH_4)_6Mo_7O_{24}$, Na_2MoO_4, WO_3 dissolved in aqueous NH_3, Na_2WO_4 and $MgSO_4$ are denoted as HT–B_4O_7, HT–PO_4, HT–Mo_7O_{24}, HT–MoO_4, HT–WO_3, HT–WO_4, and HT–SO_4, respectively. In addition to the prepared and anion–exchanged HT samples, a purchased hydrotalcite (Fujifilm Wako) denoted as HT–Wako was examined. All samples were heat treated at 773 K for 2 h in air before reaction.

2.2 Catalyst Characterization

Thermogravimetry and differential thermal analysis (TG–DTA; Rigaku TG 8120) were performed on the prepared HTs under N_2 before heat treatment to observe the thermal decomposition profiles. Powder X–ray diffraction (XRD) spectra of samples dried at 378 K and heat treated at 773 K were measured using Cu–Kα radiation (Rigaku Ultima IV). Infrared spectra were recorded on a Fourier transform spectrophotometer (JASCO FT/IR–4000), with the HTs compressed in KBr discs.

2.3 Ethanol Dehydration for Evaluation of Acidity

Ethanol dehydration into ethylene and diethyl ether, and dehydrogenation into acetaldehyde, were used as test reactions. The ethanol dehydration occurs over many acid and base catalysts. Formation of ethylene and ether is observed even on a weak acid catalyst [28]. Dehydrogenation of ethanol to acetaldehyde takes place on a solid base catalyst [28].

Ethanol conversion was carried out on the prepared catalysts in a fixed-bed flow reactor. The heat–treated catalyst (100 mg) was placed in a glass tube and pretreated at 773 K for 2 h in a He flow of 20 mL min^{-1}. The ethanol was supplied to the reactor as a saturated vapor by passing He (20 mL min^{-1}) through an ethanol trap cooled at 273 K. The saturated vapor pressure of ethanol at 273 K is 1.5 kPa. The reaction was carried out at 593 K for 3 h. Addition to the prepared catalysts, conventional SiO_2–Al_2O_3 (JRC–SAH–1) and SiO_2–MgO (JRC-SM-2) supplied by Catalysis Society of Japan were applied. The product was analyzed by gas chromatography.

3 Results and Discussion

3.1 XRD Analysis

XRD profiles of synthesized and anion–exchanged hydrotalcite samples and those treated at 773 K are shown in Figs. 1 and 2, respectively. That of purchased hydrotalcite

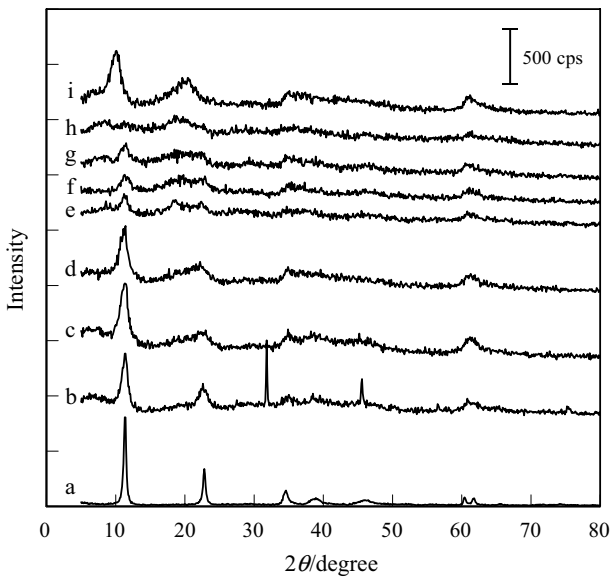

Fig. 1 XRD spectra of anion exchanged hydrotalcites. **a** HT-Wako (×5), **b** HT-Cl, **c** HT-B_4O_7, **d** HT-PO_4, **e** HT-Mo_7O_{24}, **f** HT-MoO_4, **g** HT-WO_3, **h**: HT-WO_4, **i**: HT-SO_4

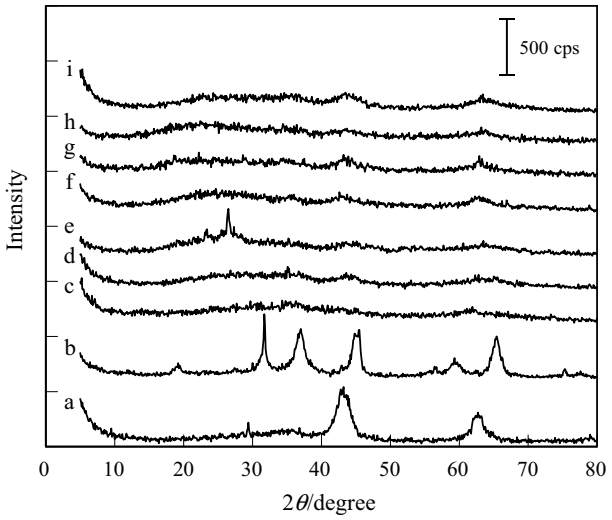

Fig. 2 XRD spectra of anion exchanged and heat treated hydrotalcites. **a** HT-Wako, **b** HT-Cl, **c** HT-B_4O_7, **d** HT-PO_4, **e** HT-Mo_7O_{24}, **f** HT-MoO_4, **g** HT-WO_3, **h**: HT-WO_4, **i**: HT-SO_4

(HT–Wako) is also shown. Characteristic diffraction peaks at $2\theta = 11.3°$ and 22.8° observed in the profile of HT–Wako in Fig. 1 were assigned to diffractions from (003) and (006) facets of typical hydrotalcite (Powder Diffraction File (PDF) No. 14–191). The lattice constants of hydrotalcite in the PDF are reported as a = b = 0.3070 nm and c = 2.323 nm. The distance between hydrogen atoms in the two layers is 0.29 nm [29]. The interlayer space is constructed by intercalated H_2O. The ionic radius of Cl^- (0.167 nm) is small enough for intercalation into the space between layers. Diffraction peaks of (003) and (006) facets are expected to shift to lower angle positions by the exchange of Cl^- with a larger anion.

All anion–exchanged HTs showed much lower peak intensities in their XRD profiles. The peak height of HT−Cl was, at most, about 20% of HT–Wako. The carbonate anion is the most suitable to form a double layered hydroxide structure. Peaks of the (003) and (006) facets in HT–Cl appeared at the same positions as those of HT−Wako. Sharp peaks at 31.9° and 45.6° were assigned to NaCl, due to incomplete washing of the sample with water.

The diffraction peak of the (003) facet of HT−B_4O_7 was in the same position as that of HT−Wako. The peak of the (006) facet had a shoulder on the lower angle side. This indicates that some Cl^- was exchanged with $B_4O_7^{2-}$, which is larger than Cl^-, resulting in expansion of the space between layers. A very similar XRD profile to HT–B_4O_7 was obtained from HT−PO_4.

In HT−Mo_7O_{24}, HT−MoO_4, and HT−WO_3, a new peak appeared around 18.5° in addition to the peak at the original position. The peak of the (006) facet at 22.3° was moved to a lower angle position by intercalation of larger oxyanions. In these samples, only partial exchange of Cl^- with the corresponding oxyanions took place. In HT−WO_4 and HT−SO_4 samples, peaks of (006) and (003) facets moved to lower angle positions and no peaks were observed at the original positions. The exchange of Cl^- took place more efficiently in these two samples.

XRD profiles of heat–treated samples are shown in Fig. 2. All samples gave low intensity and wide diffraction peaks. As shown in Fig. 1, HT−Wako possessed high crystallinity. However, the low crystallinity of the thermally decomposed product of HT–Wako was the same as the other samples. Peaks in the heat–treated HT−Wako sample at $2\theta = 43.2°$ and 62.7° were assigned to (200) and (220) facets of MgO (PDF No. 4–829), respectively. All anion–exchanged and heat–treated samples gave small and wide peaks around $2\theta = 43.2°$ and 62.7°. It can be concluded that MgO–Al_2O_3 mixed oxides prepared by anion exchange and heat treatment had the MgO structure.

A large halo in the range from 20° to 40° was observed in all samples. The halo was the clearest in the XRD profile of the HT–SO_4 sample. The halo peak is observed in solids that have lost their long–range crystalline order. Broad X–ray amorphous halos are observed in disordered nanocrystalline materials that have short–range order [30]. The angle range of the observed halo corresponded roughly to lattice spacing from 0.44 nm to 0.23 nm. The lattice constant of MgO is 0.4213 nm. The bond lengths of Mg–O and Mg–O–Mg are 0.21 nm and 0.42 nm, respectively. The observed halo could be the diffraction from a short–range order of Mg–O and Mg–O–Mg. The large halo peak in heat–treated samples indicated that heat–treated anion–exchanged samples had the MgO structure.

The small sharp peaks in the profile of HT−Mo_7O_{24} at 23.4° and 26.5° were assigned to $MgMoO_4$ (PDF No. 21 − 961). The meta–tungstate anion would be partly decomposed to ortho–tungstate. HT−Cl was converted into $MgAl_2O_4$ (PDF No. 21 − 1152) by heat treatment.

3.2 TG – DTA

Results of thermogravimetric and differential thermal analysis are summarized in Figs. 3 and 4, respectively. A continuous weight decrease without a clear stepwise weight decrease was observed in all samples except HT−Wako. A large two-step weight decrease was seen in the TG profile of HT–Wako. This is the typical TG profile of hydrotalcite ($Mg_6Al_2(OH)_{16}(CO_3)\cdot 4H_2O$) containing CO_3^{2-} as an anion in the interlayer space [27, 31, 32]. The decreasing weight in the lower temperature range was attributed to the desorption of H_2O in the interlayer space, while that in the higher temperature range was the hydroxide decomposition to oxide and CO_2 desorption.

As shown in Fig. 3, the clear stepwise decrease in sample weight nearly disappeared in prepared HTs.

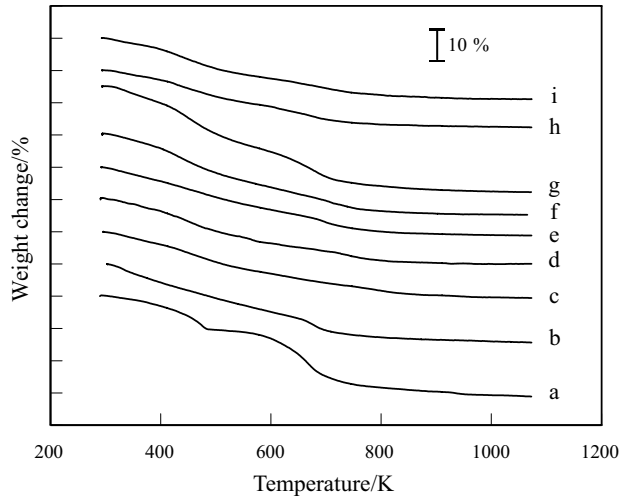

Fig. 3 Profiles of thermogravimetry analysis of anion exchanged hydrotalcites. **a** HT-Wako, **b** HT-Cl, **c** HT-B_4O_7, **d** HT-PO_4, **e** HT-Mo_7O_{24}, **f** HT-MoO_4, **g** HT-WO_3, **h**: HT-WO_4, **i**: HT-SO_4

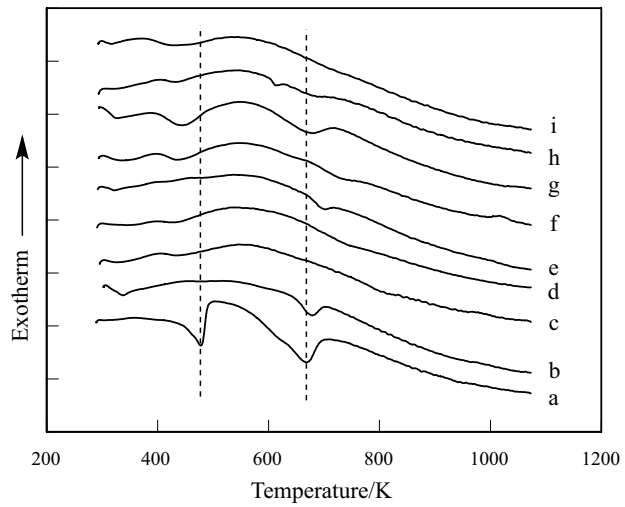

Fig. 4 Profiles of differential thermal analysis of anion exchanged hydrotalcites. **a** HT-Wako, **b** HT-Cl, **c** HT-B_4O_7, **d** HT-PO_4, **e** HT-Mo_7O_{24}, **f** HT-MoO_4, **g** HT-WO_3, **h**: HT-WO_4, **i**: HT-SO_4

The TG profiles of anion–exchanged samples were flatter than that of HT−Wako. The decreasing weight with hydroxide decomposition was barely observed in HT–Cl and HT–WO_3 samples. All samples showed a hydroxide decomposition peak at 670 K or higher as an endothermic negative peak (Fig. 4). This peak was not clear in HT–B_4O_7, HT–WO_4, and HT–SO_4 samples.

Endothermic peaks of water desorption from the interlayer space in anion-exchanged samples moved to a lower temperature range. These were separated into two parts in some samples (Fig. 4).

3.3 IR Measurements

Infrared spectra of prepared and anion-exchanged HTs were measured to confirm anion exchange by the applied procedures. IR spectra of dried samples are shown in Fig. 5. Bands from water molecules intercalated in the interlayer space and adsorbed on the surface of samples were observed in all samples around 3500 cm^{-1}. The strong wide band from 2700 to 3600 cm^{-1} was assigned to the stretching mode of the O–H bond. The band at 1632 cm^{-1} observed in all samples was assigned to adsorption of H_2O in the bending mode.

The band at 1372 cm^{-1} in HT−Wako was from the absorption by CO_3^{2-} [33]. This band disappeared in HT–Cl, demonstrating that HT–Cl had been successfully synthesized.

Broad bands appeared in the same position as carbonate in the spectrum of HT–B_4O_7. The bands between 1250 and 1500 cm^{-1} were assigned to BO_3^{3-} stretching modes [34]. The absorption band at 1074 cm^{-1} in HT−PO_4 was assigned to the P–O stretching mode [35].

HT−MoO_4 and HT−Mo_7O_{24} samples exhibited very similar IR profiles in the wavenumber region below 1300 cm^{-1}. MoO_4^{2-} was assigned to the chemical species having a band at 850 cm^{-1} [36]. The shoulder peak at 934 cm^{-1} in HT–Mo_7O_{24} was assigned to the band of $Mo_7O_{24}^{6-}$.

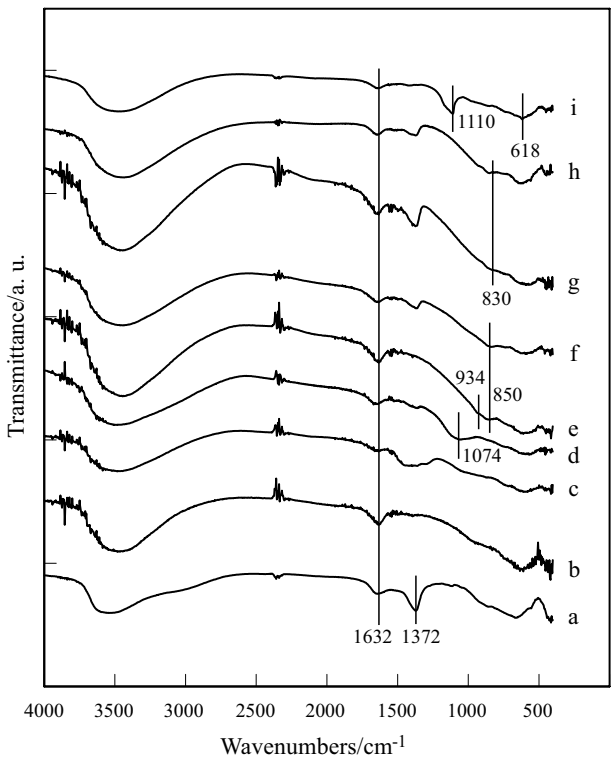

Fig. 5 IR spectra of anion exchanged hydrotalcites. **a** HT-Wako, **b** HT-Cl, **c** HT-B_4O_7, **d** HT-PO_4, **e** HT-Mo_7O_{24}, **f** HT-MoO_4, **g** HT-WO_3, **h**: HT-WO_4, **i**: HT-SO_4

MoO_4^{2-} is the most stable species among poly–molybdate anions in neutral water solution [36]. In the HT–Mo_7O_{24} sample, $Mo_7O_{24}^{6-}$ would be partially hydrated before intercalation in the interlayer space of HT.

HT–WO_3 and HT–WO_4 had spectra similar to the molybdate samples. The band at 830 cm^{-1} was assigned to WO_4^{2-} [37]. In the case of tungstate, WO_4^{2-} is the most stable in alkali solution. WO_3 was converted into $(NH_4)_2WO_4$ by dissolution in ammonia solution, which exchanged WO_4^{2-} with Cl^-. A sharp peak at 1110 cm^{-1} with a shoulder on the higher wavenumber side and a broad band at around 618 cm^{-1} observed in the HT−SO_4 sample were assigned to absorption of the SO_4 group [38].

As shown in Fig. 4, HT–Cl without carbonate was prepared successfully. Exchange of Cl^- with anions was confirmed in all exchanged samples. As shown in the XRD results in Fig. 1, the expansion of the interlayer distance was observed in HT−SO_4 and HT−WO_4 samples. It can be concluded that anion exchange of Cl^- with oxyanions was completed in these samples. XRD peaks with a wide diffraction angle range, or the appearance of a shoulder on the lower angle side, indicated that anion exchange partially took place in other samples.

3.4 Comparison of Ethanol Decomposition Activity and Selectivity

Ethanol is converted into ethylene and diethyl ether by dehydration on acid sites or acid–base pair sites. Acetaldehyde is formed by dehydrogenation on base sites. Acetaldehyde formation by oxidative dehydrogenation accompanying reduction of chemical species on the catalyst surface is also considered. The acid–base properties of the solid catalyst reflect the product selectivity [28].

The thermally decomposed product of HT–Wako was mainly composed of MgO. It was expected that the catalyst prepared from HT−Wako would show acetaldehyde selectivity to some extent due to the formation of base sites.

An enhancement of acidity was reported in metal oxides treated with oxyanions. Sulfated zirconia, prepared by introducing sulfate ion to zirconium oxide or hydroxide surface and heat treatment, is a representative example [22–24]. Introducing molybdate, tungstate, borate, and phosphate anions to the zirconia surface for acid catalyst preparation has also been studied [22–24, 39]. Therefore, solid catalysts obtained by thermal decomposition of anion–exchanged HTs were expected to have acid sites on their surfaces.

Conversion and product yields from ethanol decomposition on tested samples are shown in Table 1. All data were taken 3 h after the start of the reaction. HT–SO_4 and HT–B_4O_7 showed stable activity during the operating period, while a decrease in activity was observed in the other catalysts. The decrease in activity was particularly large in HT–Cl.

Dehydration and dehydrogenation took place on thermally decomposed HT–Wako. Formation of base sites over the MgO surface and acid sites composed of aluminum dispersed in the MgO matrix was expected in the HT–Wako sample. In HT–Cl, catalytic activity largely decreased, and acetaldehyde was not formed. Aluminates containing Sr or Ba as cations were inactive for base catalyzed retro aldol reaction of diacetone alcohol [40, 41]. $MgAl_2O_4$ found in the thermal decomposed product of HT–Cl was presumed to be inactive for base reactions, which was strongly considered as the cause for the low activity of HT–Cl. Additionally, it was considered that the remaining chloride ion formed acid sites. MgO which contained carbonate prepared by a partial thermal decomposition of basic carbonate ($Mg_5(CO_3)_4(OH)_2{\cdot}4H_2O$) showed sufficient base activity for the retro aldol reaction [42]. Acid catalyst selectivity in heat–treated HT–Cl seems to be caused by the lack of

Table 1 Ethanol dehydration over anion exchanged and heat treated hydrotalcites at 593 K

Catalyst	Conversion/%	Product Yield/%			
		Ethylene	Diethyl Ether	Acetaldehyde	Others
HT–Wako	22.4	9.2	7.6	5.6	0.0
HT–Cl	10.4	2.5	6.9	0.0	0.9
HT–PO_4	35.6	7.1	28.5	0.0	0.0
HT–B_4O_7	34.4	6.3	28.1	0.0	0.0
HT–Mo_7O_{24}	36.1	13.8	0.0	13.2	9.1
HT–MoO_4	41.6	30.8	0.0	10.7	0.0
HT–WO_3	43.7	10.3	33.4	0.0	0.0
HT–WO_4	33.8	8.7	25.0	0.0	0.0
HT–SO_4	55.9	15.5	40.4	0.0	0.0
SiO_2–MgO[a]	12.5	3.4	9.1	0.0	0.0
SiO_2–Al_2O_3[b]	47.7	10	37.7	0.0	0.0

[a]JRC–SM–2, [b]JRC–SAH-1, reaction at 503 K

carbonate in hydrotalcite, and chloride remaining in the heat–treated sample.

HT–B_4O_7, HT–PO_4, HT–WO_3, HT–WO_4, and HT–SO_4 showed higher activity and higher diethyl ether selectivity. No acetaldehyde was formed on these catalysts. Higher activity and higher ether selectivity can be attributed to acid site formation by oxyanions. The acid sites were formed by introducing oxyanions, which had an electron withdrawing effect, to several kinds of metal oxides [22–24]. There have been no reports on the formation of acid sites on MgO surfaces by introducing oxyanions. Here, acid sites would be formed by the interaction of oxyanions with alumina highly dispersed in the MgO matrix.

The catalytic activity of mixed oxides tested in this study was in similar level with SiO_2–MgO. It was much lower in comparison with that of the conventional $SiO_2–Al_2O_3$ acid catalyst. The similar dehydration activity was obtained on $SiO_2–Al_2O_3$ at the reaction temperature lowered by 90 K. The acid strength of SiO_2–MgO is the range from + 1.5 to –3.0 in Hammett function scale [43]. The acid strength of prepared catalysts was expected to be around $H_0 = 0$. The limited electron withdrawing effect of oxyanions on acid site generation was attributed to the basic environment of the MgO matrix.

Ethylene and acetaldehyde were formed on HT–Mo_7O_{24} and HT–MoO_4. Molybdate anion generated acid sites by its electron withdrawing effect [22–24]. The introduction of molybdate anion would be contributed to the acid site formation, but not to the increase of the basicity. Acetaldehyde might be formed by oxidative dehydrogenation accompanying reduction of the molybdate anion, rather than simple dehydrogenation over base sites.

4 Conclusion

Oxyanions of $B_4O_7^{2-}$, HPO_4^{2-}, $Mo_7O_{24}^{6-}$, MoO_4^{2-}, WO_4^{2-}, and SO_4^{2-} were introduced to the interlayer space of HT by anion exchange of Cl^-. In XRD analysis, shifting of peaks assigned to (006) and (003) facets to lower angle positions was observed in HT−WO_4, and HT−SO_4 samples. New peaks from these facets were found in HT−Mo_7O_{24}, HT−MoO_4, and HT−WO_3, in addition to the original peaks. A shoulder on the lower angle side of the (006) facet peak appeared in HT–B_4O_7 and HT−PO_4 samples. In IR analysis, exchanged oxyanions were detected in all of the samples. The distance between the anionic layers of hydrotalcite was expanded by the intercalation of oxyanions larger than Cl^-.

$MgO–Al_2O_3$ mixed oxides prepared by heat treatment of HT containing oxyanions at 773 K showed activity for acid catalyzed dehydration of ethanol to ethylene and diethyl ether. The effect of exchanged anions on the generation of acid sites was the largest in SO_4^{2-}. The acid sites were expected to be generated by the electron withdrawing effect of the oxyanions. The catalytic activity of $MgO–Al_2O_3$ tested in this study was much lower in comparison with that of conventional acid catalysts such as $SiO_2–Al_2O_3$. The effect of oxyanion electron withdrawing on acid site generation was expected to be limited due to the basic environment of the MgO matrix.

Acknowledgements The author would like to thank T. Satoh for technical assistance with the experiments.

Author contribution H.M. designed and implemented the research, analyzed the results, and wrote the manuscript.

Funding No funding was received to assist with the preparation of this manuscript.

Declarations

Competing interests The authors have no relevant financial or non–financial interests to disclose.

References

1. Fan G, Li F, Evans DG, Duan X (2014) Chem Soc Rev 43:7040
2. Debecker DP, Gaigneaux EM, Busca G (2009) Chem Europ J 15:3920
3. Ono Y and Hattori H (2011) Solid Base Catalysis. Springer, Heidelberg, p. 157
4. Miyata S (1983) Clays Clay Miner 31:305
5. Parker LM, Milestone NB, Newman RH (1995) Ind Eng Chem Res 34:1196
6. Theiss FL, Ayoko GA, Frost RL (2016) Appl Surf Sci 383:200
7. Kikhtyanin O, Kadlec D, Velvarská R, Kubička D (2018) Chem Cat Chem 10:1464
8. Serio MD, Ledda M, Cozzolino M, Minutillo G, Tesser R, Santacesaria E (2006) Ind Eng Chem Res 45:3009
9. Prescott HA, Li ZJ, Kemnitz E, Trunschke A, Deutsch J, Lieske H, Auroux A (2005) J Catal 234:119
10. Di Serio M, Ledda M, Cozzolino M, Minutillo G, Tesser R, Santacesaria E (2006) Ind Eng Chem Res 45:3009
11. Ebitani K, Motokura K, Mori K, Mizugaki T, Kaneda K (2006) J Org Chem 71:5440
12. Climent MJ, Corma A, Iborra S, Epping K, Velty A (2004) J Catal 225:316
13. Onda A, Ochi T, Kajiyoshi K, Yanagisawa K (2008) Catal Commun 9:1050
14. Tanabe K, Misono M, Ono Y Hattori H (1989) New Solid Acids and Bases. Kodansha-Elsevier, Tokyo
15. Di Cosimo JI, Díez VK, Xu M, Iglesia E, Apesteguía CR (1998) J Catal 178:499
16. Yamaguchi K, Ebitani K, Yoshida T, Yoshida H, Kaneda K (1999) J Am Chem Soc 121:4526
17. Corma A, Fornés V, Martín-Aranda RM, Rey F (1992) J Catal 134:58
18. Nakatsuka T, Kawasaki H, Yamashita S, Kohjiya S (1979) Bull Chem Soc Jpn 52:2449
19. Angelici C, Velthoen MEZ, Weckhuysen BM, Bruijnincx PCA (2015) Catal. Sci Technol 5:2869

20. Matsuhashi H, Nagashima K, Naijo N, Aritani H (2010) Top Catal 53:659
21. Sakamoto Y, Matsuhashi H, Nakamura H (2011) J Jpn Petrol Inst 54:385
22. Arata K, Matsuhashi H (2011) Solid Superacids. Nove Science Publishers, New York
23. Arata K (2009) in Metal Oxide Catalysis, Vol. 2, ed. Jackson SD, Hargreaves JSJ. Wiley-VCH, Weinheim, p. 665
24. Arata K (1990) Adv Catal 37:165
25. Tichit D, Bennani MN, Figueras F, Tessier R, Kervennal J (1998) Appl Clay Sci 13:401
26. Tsujimura A, Uchida M, Okuwaki A (2007) J Hazard Mater 143:582
27. Zhang J, Xu YF, Qian G, Xu ZP, Chen C, Liu Q (2010) J Phys Chem C 114:10768
28. Phung TK, Busca G (2015) Chem Eng J 272:92
29. Pérez-Ramírez J, Abelló S, van der Pers NM (2007) Chem Eur J 13:870
30. Bates S, Zografi G, Engers D, Morris K, Crowley K, Newman A (2006) Pharmac Res 23:2333
31. Kanezaki E (1998) Solid State Ionics 106:279
32. Vágvölgyi V, Palmer SJ, Kristóf J, Frost RL, Horváth E (2008) J Coll Inter Sci 318:302
33. Roelofs JCAA, van Bokhoven JA, Jos van Dillen A, Geus JW, de Jong KP (2002) Chem Eur J 8:5571
34. Shi L, Li D, Wang J, Li S, Evans DG, Duan X (2005) Clays Clay Miner 53:294
35. Ye L, Qu B (2008) Poly Degrad Stabil 93:918
36. Davanteès A, Lefeèvre G (2013) J Phys Chem A 117:12922
37. Davanteès A, Costa D, Lefeèvre G (2015) J Phys Chem C 119:12356
38. Sato M, Kuwabara H, Saito S (1992) Clay Sci 8:309
39. Segawa K, Nakata S, Asaoka S (1987) Mater Chem Phys 17:181
40. Matsuhashi H, Sato K, Misu S, Yoshida K (2020) J Jpn Petro Inst 63:20
41. Matsuhashi H, Iwamoto A, Sasaki M, Yoshida K, Aritani H (2021) J Jpn Petrol Inst 64:103
42. Kitagawa M, Ishida N, Yoshino E, Matsuhashi H (2020) Res Chem Intermed 46:3703
43. Benesi HA (1956) J Am Chem Soc 78:5490